JOURNAL OF GEOPHYSICAL RESEARCH, VOL. 115, C07017, doi:10.1029/2009JC006073, 2010

Heat and salt balances over the New England continental shelf, August 1996 to June 1997

S. J. Lentz,[1] R. K. Shearman,[2] and A. J. Plueddemann[1]

Received 21 December 2009; revised 20 March 2010; accepted 1 April 2010; published 29 July 2010.

[1] Heat and salt balances over the New England shelf are examined using 10 month time series of currents, temperature, and salinity from a four element moored array and surface heat and freshwater fluxes from a meteorological buoy. A principal result is closure of the heat budget to 10 W m^{-2}. The seasonal variation in depth-average temperature, from 14°C in September to 5°C in March, was primarily due to the seasonal variation in surface heat flux and a heat loss in winter caused by along-shelf advection of colder water from the northeast. Conductivity sensor drifts precluded closing the salt balance on time scales of months or longer. For time scales of days to weeks, depth-average temperature and salinity variability were primarily due to advection. Advective heat and salt flux divergences were strongest and most complex in winter, when there were large cross-shelf temperature and salinity gradients at the site due to the shelf-slope front that separates cooler, fresher shelf water from warmer, saltier slope water. Onshore flow of warm, salty slope water near the bottom and offshore flow of cooler, fresher shelf water due to persistent eastward (upwelling-favorable) winds caused a temperature increase of nearly 3°C and a salinity increase of 0.8 in winter. Along-shelf barotropic tidal currents caused a temperature decrease of 1.5°C and a salinity decrease of 0.7. Wave-driven Stokes drift caused a temperature increase of 0.5°C and a salinity increase of 0.4 from mid December to January when there were large waves and large near-surface cross-shelf temperature and salinity gradients.

Citation: Lentz, S. J., R. K. Shearman, and A. J. Plueddemann (2010), Heat and salt balances over the New England continental shelf, August 1996 to June 1997, *J. Geophys. Res.*, *115*, C07017, doi:10.1029/2009JC006073.

1. Introduction

[2] The objective of this study is to determine the processes contributing to temperature and salinity variability over time scales of days to a year on the New England shelf. Of particular interest is the relative importance of advection and the specific advective processes that cause substantial variations in the depth-average temperature and salinity. Temperature and salinity are important to shelf dynamics because they determine the density distribution which is a key element of shelf dynamics. Additionally, understanding processes controlling temperature and salinity variability provide insight into important advective pathways that are likely to influence distributions of other constituents, such as nutrients.

[3] Water temperatures on the New England shelf undergo a large seasonal variation, with depth-averaged temperatures at mid-shelf ranging from a maximum of about 12°C in late summer to a minimum of about 5°C in late winter [*Bigelow*, 1933; *Mayer et al.*, 1979; *Beardsley et al.*, 1985; *Lentz et al.*, 2003a]. This seasonal variation is qualitatively consistent with the seasonal variation in surface heat flux, i.e., surface warming in spring and summer and surface cooling in fall and winter [*Beardsley and Boicourt*, 1981; *Joyce*, 1987; *Mountain et al.*, 1996; *Beardsley et al.*, 2003]. However, the relative importance of advection to the seasonal variation in temperature, and to temperature variability in general, remains unclear because few observational studies have provided accurate estimates of the horizontal temperature gradients.

[4] There have been only a few quantitative studies of the heat balance over the Middle Atlantic Bight (MAB) continental shelf. *Lentz et al.* [2003b] used a 6-month moored array deployment to examine the heat balance at mid-shelf on the southern flank of Georges Bank, to the northeast of the New England shelf. They found that the seasonal increase in temperature from February to August 1995 was primarily due to surface heating while advective heat fluxes dominated the temperature variability over time scales of days to weeks. There have been several direct estimates of the cross-shelf eddy heat flux at the shelf-slope front which indicate that the onshore heat flux at the front is small relative to the surface heat flux [*Houghton et al.*, 1988, 1994; *Garvine et al.*, 1989; *Gawarkiewicz et al.*, 2004]. *Bignami and Hopkins* [2003] inferred from surface heat fluxes and temperature changes that advective heat fluxes at the southern end of the Middle Atlantic Bight, near Cape Hatteras, must be large. Recently, *Lentz* [2010] used historical data to show that surface heat fluxes and along-shelf advection could account for the

[1]Department of Physical Oceanography, Woods Hole Oceanographic Institution, Woods Hole, Massachusetts, USA.
[2]College of Oceanic and Atmospheric Sciences, Oregon State University, Corvallis, Oregon, USA.

0148-0227/10/2009JC006073

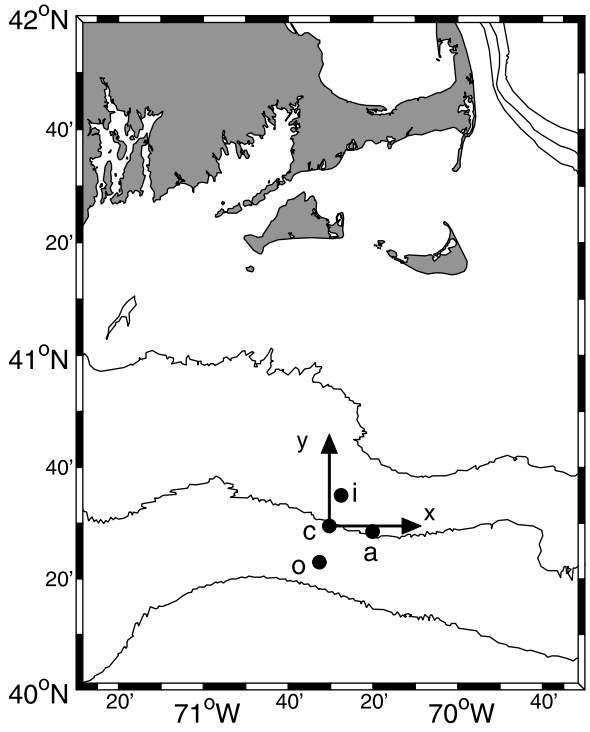

Figure 1. Map showing locations of the inshore (i), central (c), offshore (o), and alongshore (a) sites on the New England shelf south of Cape Cod and the orientation of the *x*, *y* coordinate frame, *x* is positive toward the east. The along-shelf site is located 8° clockwise from the *x* axis and the inshore and offshore sites are 20° and 15° clockwise from the *y* axis. The 50-m, 70-m, and 100-m isobaths are also shown.

observed along-isobath temperature increase from northeast to southwest in the MAB. However, this result was sensitive to the uncertainty in the surface heat flux climatologies. Several studies of the heat balance over the MAB inner shelf indicate that cross-shelf advection (upwelling) tends to balance surface heating over the inner-shelf in summer when thermal stratification is strong, but that cooling and possibly along-shelf advection dominate the inner-shelf heat balance in winter when thermal stratification is weak [*Austin and Lentz*, 1999; *Wilkin*, 2006; *Fewings*, 2007]. Only the Georges Bank measurements were sufficient to directly estimate the terms in the local heat balance at mid shelf and that study only spanned half the annual cycle.

[5] In contrast to temperature, the seasonal variation in salinity on the New England shelf is small compared to either shorter time scale variations or inter-annual variations [*Manning*, 1991]. There is a slight freshening of the New England shelf water in spring, presumably associated with increased freshwater runoff in the Gulf of Maine and farther north [*Bigelow and Sears*, 1935; *Manning*, 1991], and possibly to local runoff from the southern coast of New England, notably the Connecticut River [*Lentz et al.*, 2003a]. Salinity variations on the shelf are assumed to be primarily due to advection, since evaporation minus precipitation is small [*Beardsley and Boicourt*, 1981; *Joyce*, 1987]. Potentially important contributions to salinity variability on the New England shelf include along-shelf advection of freshwater runoff and cross-shelf displacements of the shelf-slope front that separates the relatively fresh shelf water from saltier slope water [e.g., *Bigelow and Sears*, 1935; *Manning*, 1991; *Linder and Gawarkiewicz*, 1998; *Lentz et al.*, 2003a].

[6] There have been a number of estimates of the volume salt budget for the MAB aimed at determining the cross-shelf flux of salt at the shelfbreak [*Wright*, 1976; *Fairbanks*, 1982; *Brink*, 1998; *Bignami and Hopkins*, 2003], as well as, a few direct estimates of the cross-shelf salt flux at the shelf break [*Garvine et al.*, 1989; *Gawarkiewicz et al.*, 2004]. These studies suggest there is an onshore flux of salt at the shelf break but the magnitude is poorly constrained. However, there has been only one study that provided direct estimation of the terms in the local salt balance in the region, the study on the southern flank of Georges Bank [*Lentz et al.*, 2003b]. They found that salinity variations were dominated by advection, notably movement of saltier slope water onto the southern flank of Georges Bank.

[7] In this study, the depth-averaged heat and salt balances over the New England shelf are examined using observations from a moored array deployed at mid-shelf that spans almost a full year (August 1996 to June 1997) as part of the Coastal Mixing and Optics program (CMO). The moored array observations included a suite of meteorological measurements that provide direct estimates of the surface heat and freshwater fluxes, as well as, temperature, salinity (from conductivity and temperature), and current observations that allow estimation of the horizontal advective fluxes and the changes in temperature and salinity. Surface gravity wave measurements also allow estimation of the heat and salt flux due to the wave-driven Stokes drift [*Fewings*, 2007].

[8] *Lentz et al.* [2003a] found that water temperatures during CMO were similar to monthly means based on historical hydrographic data except near the bottom where temperatures were colder than historical means in fall and warmer than historical means in winter. This suggests the processes contributing to the heat balance during CMO are probably typical for this region. The CMO salinities were substantially fresher (0.5–1, practical salinity scale) than normal. Similar anomalies were also observed during 1996–1997 north of the New England shelf suggesting the anomalously low salinities were a large-scale phenomenon [*Benway and Jossi*, 1998; *Smith et al.*, 2001]. This suggests the processes contributing to the salt balance during CMO may not be typical for this region, at least for time scales of months or longer.

2. Observations and Analysis

2.1. Moored Array and Data Processing

[9] The CMO moored array consisted of four sites located on the outer half of the New England continental shelf south of Cape Cod, Massachusetts [*Lentz et al.*, 2003b; *Shearman and Lentz*, 2003]. A heavily instrumented central site on the 70-m isobath was surrounded by three more lightly instrumented sites, an inshore site 11 km onshore of the central site in 64 m of water, an offshore site 12.5 km offshore of the central site in 86 m of water, and an alongshore site 14.5 km east of the central site in 69 m of water (Figure 1).

[10] Temperature, conductivity, and current observations spanning the water column were obtained from instruments deployed on surface/subsurface mooring pairs at each site.

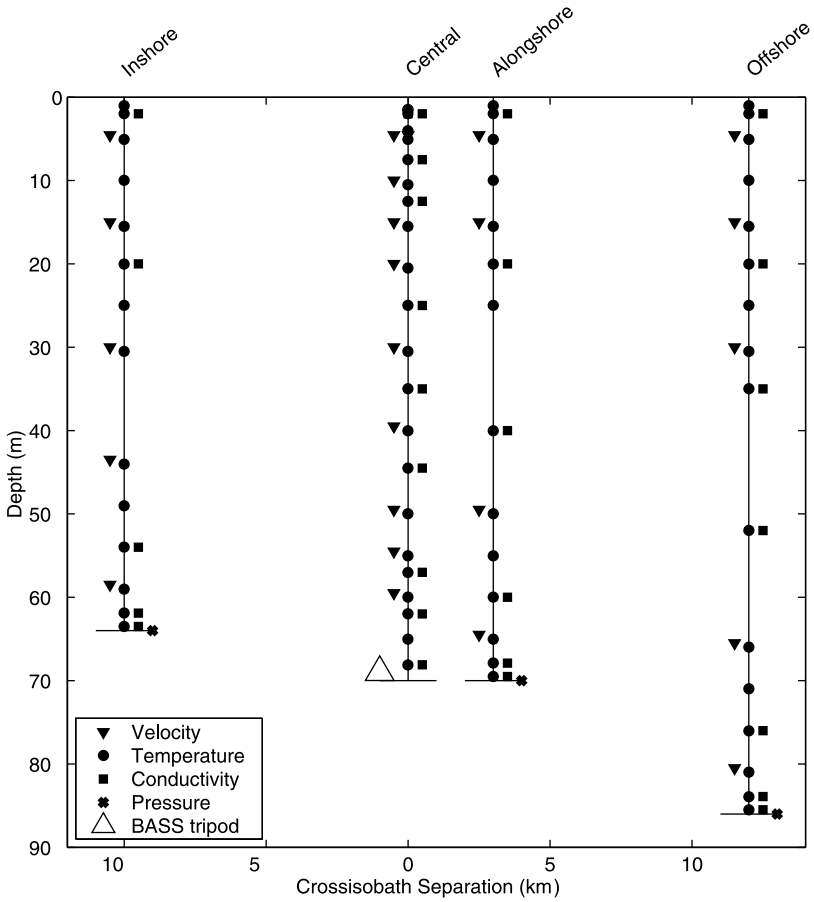

Figure 2. Schematic of the subsurface moored instrumentation.

Vector-Measuring Current Meters (VMCMs) were used to measure horizontal velocity and temperature, and SeaBird SeaCats to measure temperature and conductivity. The VMCMs were designed to accurately average near-surface velocities in the presence of surface wave motion [*Weller and Davis*, 1980]. Vertical spacing of temperature measurements was 3–5 m at the central site and 5–10 m at the surrounding sites (Figure 2). Vertical spacing of current and conductivity measurements were approximately every 5 m at the central site and 10 m at the surrounding sites. Meteorological observations from the central site buoy included wind speed and direction, air temperature, near-surface water temperature, relative humidity, incoming short and long-wave radiation, atmospheric pressure, and precipitation. Surface gravity wave spectra were obtained from a SeaTex waverider buoy deployed at the central site.

[11] *Galbraith et al.* [1999] and *Shearman and Lentz* [2003] provide detailed descriptions of the moored array, instrumentation, and initial data processing. Estimated accuracies are 0.02–0.03 m s^{-1} for currents including wave-biases [*Beardsley*, 1987], 0.05°C for temperature, and 0.15 for salinity (see section 2.4). There are gaps of 9 and 25 days during the fall in the near-surface observations from the inshore and alongshore sites respectively due to mooring failures. Failures in the mooring tether for the waverider buoy resulted in data gaps from 5 to 25 September 1996 and from 7 February to 16 April 1997. These gaps were fill with observations of significant wave height and wave period from adjacent NDBC buoys. Dominant wave direction was not available from the NDBC buoys, so the gaps were filled with the average wave direction from the waverider buoy (13° clockwise from N). Correction of offsets, abrupt jumps, and drifts in the conductivity time series due to fouling are discussed briefly in section 2.4, see *Galbraith et al.* [1999] for a detailed description.

[12] Sampling intervals were 7.5 minutes or shorter for most of the instrumentation. Time series were low-pass filtered to remove variability having time scales shorter than an hour and decimated to hourly values to form a common time base. An along- and cross-shelf coordinate frame aligned with the mean depth-averaged flow is adopted with x positive, eastward, toward 90°T and y positive onshore, northward toward 0°T (Figure 1). The local isobaths and the principal axes of the subtidal flow are oriented about 20° clockwise from eastward.

2.2. Depth-Average Temperature and Salt Balances

[13] The depth-averaged temperature and salinity balances are

$$\langle T\rangle_t + \langle uT_x\rangle + \langle vT_y\rangle + \langle wT_z\rangle = \frac{Q}{\rho_o C_P h} \qquad (1)$$

and

$$\langle S\rangle_t + \langle uS_x\rangle + \langle vS_y\rangle + \langle wS_z\rangle = -\frac{(P-E)S_{ref}}{h}, \qquad (2)$$

where T is temperature, S is salinity, t is time, u, v, and w are the along-shelf, cross-shelf and vertical components of velocity, $\langle\rangle$ indicates the depth-average from the surface to the bottom, t, x, y, and z subscripts imply differentiation, Q is the surface heat flux, $\rho_o = 1025$ kg m^{-3} is a reference density, $C_P = 4190$ W kg^{-1}°C^{-1} is the heat capacity of sea water, P is the precipitation rate and E is the evaporation rate (both in m s^{-1}), $S_{ref} = 32$ is a reference salinity (approximately the mean salinity), and h is the water depth (70 m at the central site). Fluxes of heat and salt through the sea floor are assumed to be negligible. All of the terms in (1) and (2) can be estimated using the available observations (as described below) except the vertical advective flux terms $\langle wT_z\rangle$ and $\langle wS_z\rangle$. Rough estimates assuming $w \approx uh_x$ suggest these terms are generally small, but they could be significant during periods when vertical temperature and salinity gradients are large. The vertical advective fluxes are not considered in the subsequent analysis.

[14] To focus on the observed temperature and salinity variability and to emphasize longer time scales, (1) and (2) are integrated in time from the start of the time series ($t = 0$) to get

$$\langle T\rangle = T_o + Q^{cum} - FT \qquad (3)$$

and

$$\langle S\rangle = S_o + PE^{cum} - FS, \qquad (4)$$

where $T_o = \langle T(t=0)\rangle$, $S_o = \langle S(t=0)\rangle$,

$$Q^{cum} = \int_0^t \frac{Q}{\rho_o C_P h}dt, \text{ and } PE^{cum} = -\int_0^t \frac{(P-E)S_{ref}}{h}dt$$

are the cumulative surface heat and freshwater fluxes, and

$$FT = \int_0^t (\langle uT_x\rangle + \langle vT_y\rangle)dt$$

and

$$FS = \int_0^t (\langle uS_x\rangle + \langle vS_y\rangle)dt$$

are the cumulative horizontal advective heat and salt fluxes.

[15] It will be shown in section 3.4 that tidal variability and surface gravity waves make significant contributions to the subtidal advective heat and salt fluxes. To separate the contributions of subtidal and tidal (and other high frequency) variability to the advective fluxes, the current, temperature gradient and salinity gradient time series are decomposed into low-frequency (periods longer than 38 hours) and high-frequency (periods between 38 and 2 hours) components, e.g., $u = u^{lf} + u^{hf}$. The hourly time series of each variable were low-pass filtered using PL64 [*Beardsley et al.*, 1985], which has a half-power point of 38 hours, to estimate the low-frequency time-series. The high-frequency time series were then calculated by subtracting the low-frequency time series from the original hourly time series, e.g., $u^{hf} = u - u^{lf}$. The cumulative advective heat flux contributions from the low-frequency and high-frequency variability are

$$FT^{lf} = \int_0^t \langle u^{lf}T_x^{lf}\rangle + \langle v^{lf}T_y^{lf}\rangle dt$$

and

$$FT^{hf} = \int_0^t \langle u^{hf}T_x^{hf}\rangle + \langle v^{hf}T_y^{hf}\rangle dt.$$

The cross-term contributions, e.g., $u^{lf}T_x^{hf}$, though not identically zero because of the finite record length and imperfect filter, are negligible, less than 0.3% of the variance of FT^{lf} or FT^{hf}.

[16] The current, temperature, and conductivity sensors did not sample fast enough to resolve surface gravity waves. However, the temperature and salt flux due to covariance of surface gravity wave current and temperature (or salinity) variability can be estimated from the associated Stokes drift velocity (u^{st}, v^{st}) and the observed temperature or salinity gradients as $u^{st}T_x + v^{st}T_y$ [*Fewings*, 2007]. The Stokes velocities were estimated from the significant wave height H_{sig}, the wave period T_p and the wave direction θ_w as

$$(u^{st}, v^{st}) = \frac{H_{sig}^2\omega k}{16}\frac{\cosh(2k[z+h])}{\sinh^2(kh)}(\cos(\theta_w), \sin(\theta_w)), \qquad (5)$$

where ω is the frequency corresponding to the dominant wave period, and k is the magnitude of the wave number determined from the dispersion relation for linear surface gravity waves. Thus, the cumulative advective heat flux due to surface gravity waves is

$$FT^{st} = \int_0^t \langle u^{st}T_x\rangle + \langle v^{st}T_y\rangle dt.$$

The resulting cumulative heat balance is

$$\langle T\rangle = T_o + Q^{cum} - FT^{lf} - FT^{hf} - FT^{st} \qquad (6)$$

and the corresponding cumulative salt balance is

$$\langle S\rangle = S_o + PE^{cum} - FS^{lf} - FS^{hf} - FS^{st}. \qquad (7)$$

2.3. Estimation of Terms in the Temperature and Salt Balances

[17] Estimates of the terms in the temperature and salt balances are centered on the central site ($h = 70$ m). Depth-averages are estimated using a trapezoidal rule, extrapolating to the surface or bottom by assuming variables are vertically uniform near the boundaries. Current measurements were typically within 5 m of the surface and bottom and temperature and conductivity measurements were within 1–2 m (Figure 2). Time derivatives are estimated as centered, finite differences over two-hour intervals.

[18] Surface heat flux, evaporation, and wind stress were estimated from the meteorological measurements using bulk formulas [*Fairall et al.*, 1996]. Horizontal advective fluxes are estimated using the velocity at the central site and estimating horizontal temperature and salinity gradients using observations from all four mooring sites. The temperatures

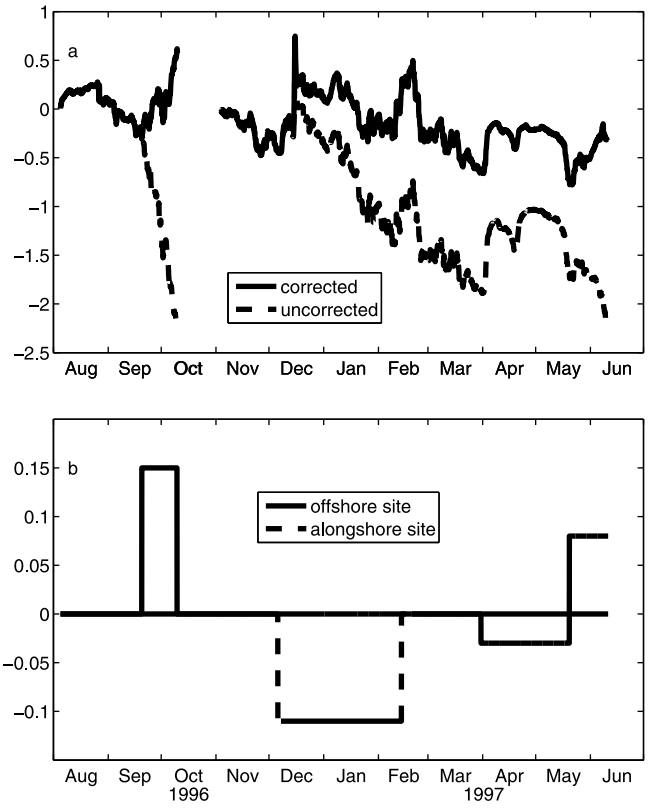

Figure 3. Time series of (a) the corrected (solid) and uncorrected (dashed) cumulative advective salt flux and (b) the vertically uniform offsets applied to the salinities at the offshore (solid) and alongshore (dashed) sites to generated the "corrected" salt flux time series in Figure 3a.

and salinities at each site were interpolated to the depths of the current observations at the central site. The mooring sites were not exactly aligned with the x, y coordinate axes, the along-shelf site was 8° clockwise from the x axis and the inshore and offshore sites are 20° and 15° clockwise from the y axis (Figure 1). Therefore, horizontal temperature and salinity gradients were estimated by fitting a plane to the vertically interpolated temperatures or salinities at each depth for each hour and then estimating the horizontal gradients along the x and y axes. Use of a quadratic fit in the cross-shelf direction, since there are three moorings, does not substantially improve the closure of the heat and salt balances.

2.4. Salinity Offsets

[19] The conductivity time series exhibited offsets, abrupt jumps, and drifts due to fouling that were identified and corrected (to the extent possible) by comparisons with adjacent instruments on the same mooring and shipboard CTD casts near the moorings [*Galbraith et al.*, 1999]. The offsets and drifts are more severe near the bottom and are likely due to suspended sediment fouling the conductivity cell rather than bio-fouling. Inaccuracies in our initial correction of the conductivity time series are almost certainly the cause of large drifts in the cumulative advective salt flux FS (Figure 3a, dashed line) that are inconsistent with other terms in the cumulative salt balance (discussed in section 3.3.3). These offsets are small relative to the salinity variability, but the resulting inaccuracies in the salinity gradient estimates result in large drifts in the cumulative advective salt flux.

[20] Ad hoc time-dependent, depth-independent salinity offsets of 0.15 or less, chosen to minimize the discrepancy in the cumulative salt balance, were applied to the salinity time series from the offshore and alongshore sites (Figure 3b). These small offsets (Figure 3b) are sufficient to remove the large drifts in the advective salt flux (Figure 3a, solid line) and are applied in the subsequent analyzes to facilitate examination of the salt balance. Application of these ad hoc offsets means that salt balance results for time scales longer than weeks are only qualitative, but does not change the variability, or affect the interpretation of results, on time scales of days to weeks.

3. Results

3.1. Wind Stress, Surface Gravity Waves, and Currents

[21] Wind stress primarily varies on time scales of days associated with the passage of storms and atmospheric fronts (Figure 4a). Peak wind stresses during storms are typically 0.4 Pa, with a maximum of almost 1 Pa when hurricane Edouard passed 100 km to the east of the moored array on 4 September. Significant wave heights are correlated with

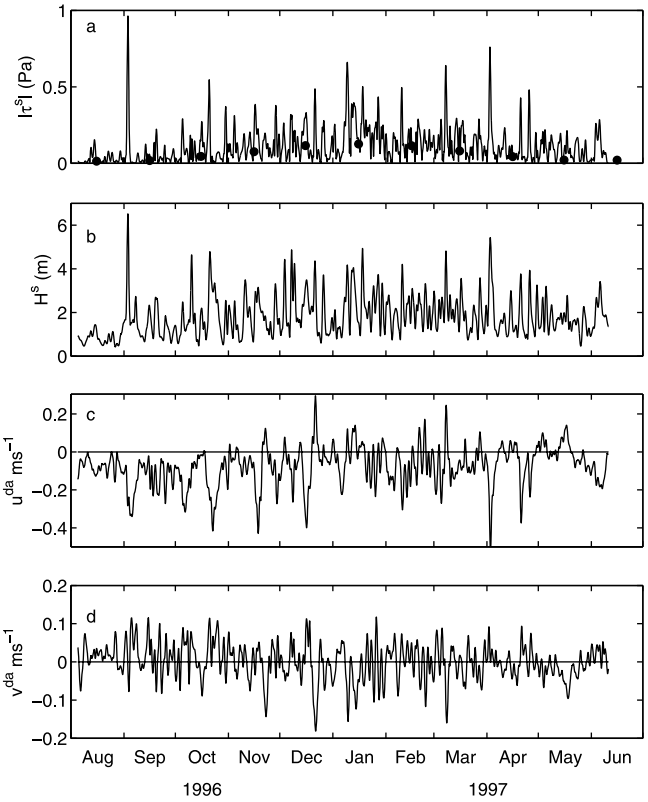

Figure 4. Time series of the (a) wind stress magnitude $|\tau^s|$, (b) significant wave height H_s, (c) depth-average along-shelf velocity, and (d) depth-average cross-shelf velocity at the central site. Monthly mean wind stress magnitudes from NCEP reanalysis averaged over the period 1948–2000 for a 2 degree grid square centered on 41°N 71.25°W are also shown (circles) in Figure 4a.

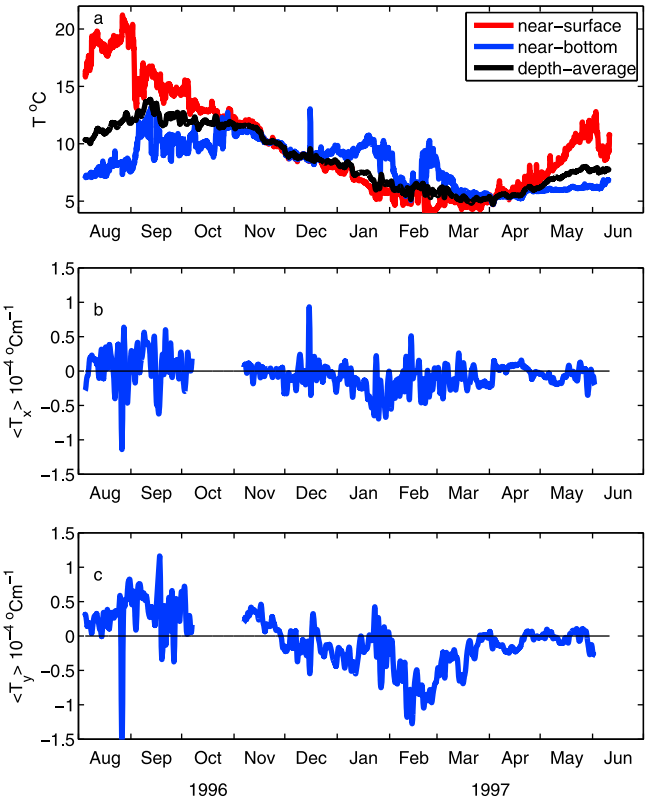

Figure 5. Time series of (a) the near-surface (red), near-bottom (blue), and depth-average (black) temperature and the depth-average (b) along-shelf ($\langle T_x \rangle$) and (c) cross-shelf ($\langle T_y \rangle$) temperature gradients at the central site.

wind stress magnitude, with peak values of 3–5 m during storms (Figure 4b). The dominant wave direction tends to be onshore and peak wave periods are typically 6–12 s. Wind stresses and waves are larger in fall and winter and smaller in summer and spring.

[22] Subtidal currents are polarized along-shelf, with depth-average along-shelf currents ranging from −0.5 to 0.3 m s^{-1} and depth-average cross-shelf currents generally less than 0.1 m s^{-1} in magnitude (Figures 4c and 4d) [*Beardsley et al.*, 1985; *Shearman and Lentz*, 2003]. Depth-average along-shelf currents consist of events lasting days to weeks that are typically westward, with only a few notable eastward current events in winter (Figure 4c). The mean, depth-average cross-shelf current is zero because along-shelf is defined as aligned with the mean depth-averaged current. Tidal currents are predominantly semi-diurnal with an amplitude of about 0.1 m s^{-1} [*Shearman and Lentz*, 2004] and episodic near-inertial currents with rms velocities up to 0.1 m s^{-1} occur during stratified periods [*Shearman*, 2005].

3.2. Temperature

3.2.1. Water Temperature Temporal Variability and Structure

[23] Water temperatures at the central site during the CMO deployment exhibit a large annual variation that is consistent with the typical annual cycle over the New England shelf [*Beardsley and Boicourt*, 1981; *Lentz et al.*, 2003a]. The depth-average temperature at the central site rises from 10°C in early August to a maximum of about 14°C in mid September, decreases through the fall and winter to a minimum of 5°C in mid March, and then, beginning in early April, rises again to 8°C in late May (Figure 5a, black line). A similar annual variation was observed at all four sites.

[24] There is a large vertical variation in temperature in August (seasonal thermocline), with warm water (>18°C) in the upper 20 m and cooler water (<10°C) in the lower 50 m separated by a sharp thermocline (Figure 5a, red and blue lines). The vertical temperature difference decreases to approximately zero by November in response to several storms [*Lentz et al.*, 2003a]. Water temperatures continue to decrease through winter. Near the bottom there is a fairly persistent temperature inversion (near-bottom water warmer than near-surface water) from mid December to March. This warmer near-bottom water is associated with the onshore movement of the foot of the shelf-slope front that separates cooler, fresher shelf water from warmer, saltier slope water [*Linder and Gawarkiewicz*, 1998]. The seasonal thermocline redevelops in spring as near-surface waters warm.

[25] The depth-average along-shelf and cross-shelf temperature gradients $\langle T_x \rangle$, $\langle T_y \rangle$ are variable on time scales of days to months (standard deviations of 2.5×10^{-5} and 4×10^{-5} °C m^{-1}) (Figures 5b and 5c). The mean along-shelf and cross-shelf temperature gradients (-0.5×10^{-5} °C m^{-1} and -0.6×10^{-5} °C m^{-1} respectively), are both small relative to the variability, with warmer water to the west and offshore. However, $\langle T_y \rangle$ exhibits a substantial seasonal variation with a positive gradient ($\approx 5 \times 10^{-5}$ °C m^{-1}, warmer water onshore) from August to November and a negative gradient ($\approx -5 \times 10^{-5}$ °C m^{-1}) from December to March, and a near-zero cross-shelf gradient during April and May (Figure 5c). This seasonal variation in $\langle T_y \rangle$ is qualitatively consistent with the tendency for surface heating in summer to increase temperatures in shallow water more than in deep water and surface cooling in winter to decrease water temperatures in shallow water more than in deep water [*Shearman and Lentz*, 2003].

3.2.2. Surface Heat Flux

[26] The net surface heat flux exhibits a large seasonal variation (Figure 6a). In the summer and spring (August to September and April to June), there is a positive (into the ocean) surface heat flux of 100–200 W m^{-2} due to incoming solar radiation (Figure 6b) and small latent and sensible heat losses (Figure 6c). In fall, the net surface heat flux decreases, as solar radiation decreases and cooling due to latent and sensible heat loss increases. In winter (November–January), solar heating is relatively small ($\approx$50 W m^{-2}) and latent and sensible heat losses are large (up to 200 W m^{-2} for each). The large (<-100 W m^{-2}) latent and sensible heat loss events in winter are typically associated with south-eastward winds that bring cold, dry air from the continent over the shelf. There is a relatively constant heat loss of about −50 W m^{-2} due to the net long-wave radiation (Figure 6b). The monthly means from the NCEP Reanalysis indicate that the seasonal variation in surface heat flux during the CMO deployment period was fairly typical.

3.2.3. Heat Balance

[27] The cumulative heat balance is examined by comparing the right-hand and left-hand sides of (6). The sum of the cumulative surface and advective heat fluxes (Figure 7a, red line) matches both the seasonal variation and most of the

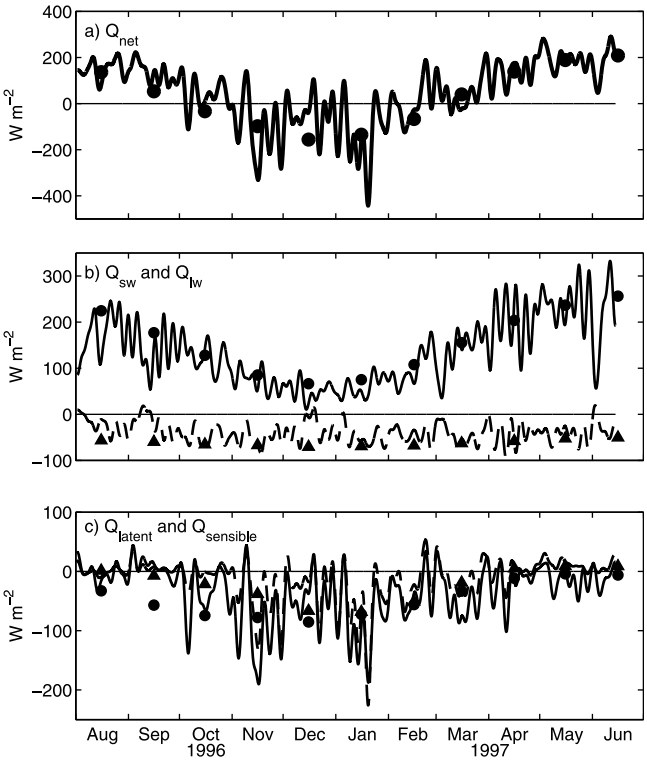

Figure 6. Time series of the (a) net surface heat flux Q_{net}, (b) short-wave Q_{sw} (solid line, circles) and long-wave Q_{lw} (dashed line, triangles) heat fluxes, and (c) latent Q_{latent} (solid line, circles) and sensible $Q_{sensible}$ (dashed line, triangles) heat fluxes. Lines are estimates from CMO central site and symbols are monthly means of the surface heat flux components from NCEP reanalysis averaged over the period 1948–2000 for a 2 degree grid square centered on 41°N 71.25°W.

shorter time scale variations in the depth-average temperature at the central site (Figure 7a, blue line). The correlation between the cumulative heat fluxes and the observed depth-average temperature is 0.97. The correlation is 0.67 (significant at the 95% confidence level) if the annual cycle is removed from both time series. The overall agreement is equivalent to closing the mean heat balance over 10 months to within about 10 W m^{-2}. This remarkable agreement indicates: 1) the meteorological observations and the bulk formula are yielding accurate surface heat flux estimates and 2) the moored array is resolving the dominant scales contributing to advective heat fluxes. Thus, the surface and advective heat flux estimates are accurate enough to determine the dominant processes contributing to variations in the depth-averaged temperature.

[28] Advective heat flux divergences are the dominant cause of depth-averaged temperature variations on time scales of days to weeks (Figure 7b, blue line), whereas the cumulative surface heat flux shows little variation on those time scales (Figure 7b, red line). This is also evident from examination of the subtidal heat balance (1) (not shown), which emphasizes shorter time scales than the cumulative heat balance. The dominant terms in the subtidal heat balance are temporal changes in temperature (T_t) and the advective heat flux divergence ($uT_x + vT_y$) (correlation −0.55, regression slope −0.4 ± 0.07).

[29] Over seasonal time scales the contributions of the surface heat flux and horizontal advective heat flux are similar in magnitude (Figure 7b). The surface heat flux warms the water column during August and September, cools the water column from November to January, and warms the water column during April and May. The cumulative advective heat fluxes produce a temperature increase during the late summer (August to mid September) that is about the same magnitude as the surface heat flux contribution over this period. The advective heat flux causes little net change in depth-average temperature during the fall (mid September to December), a fairly steady temperature decrease of about 5°C over the winter (December–March), and essentially no change in temperature during the spring (April and May). The contributions of subtidal, tidal, and surface gravity wave variability to the advective heat (and salt) flux divergence are examined in section 3.4.

3.3. Salinity

3.3.1. Salinity Temporal Variability and Structure

[30] In contrast to water temperature, depth-averaged salinity at the central site does not exhibit an obvious seasonal variation. Instead, the dominant variability has time scales of days to months with depth-average salinities ranging between 31.6 and 32.6 (Figure 8a, black line).

[31] Salinities increase with water depth. Near surface salinities range from 31.5 to 32 and near-bottom salinities

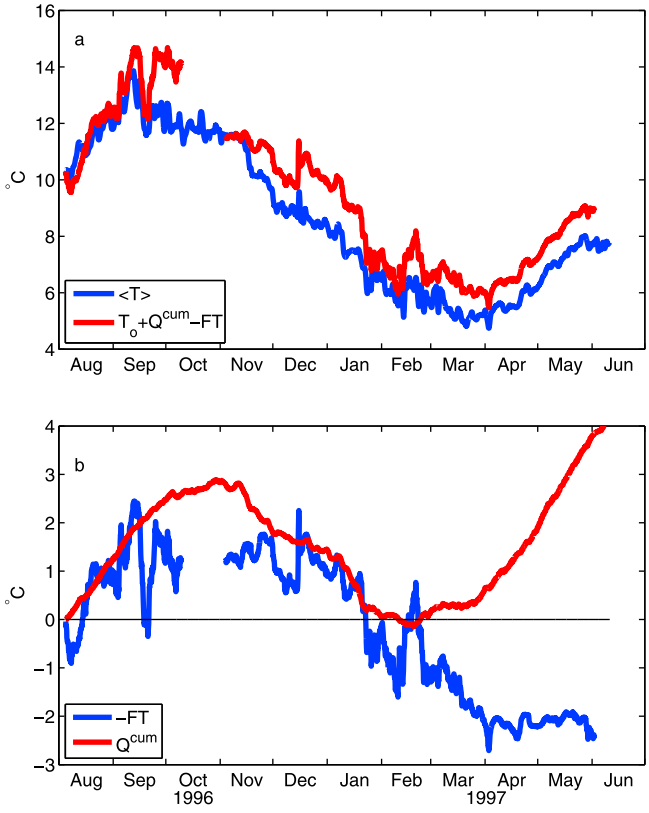

Figure 7. Time series of (a) the depth-averaged temperature ($\langle T \rangle$) at the central site (blue line) and the cumulative surface plus advective heat flux divergence (red line) and (b) the cumulative advective heat flux divergence $-FT$ (blue line) and the cumulative surface flux Q^{cum} (red line).

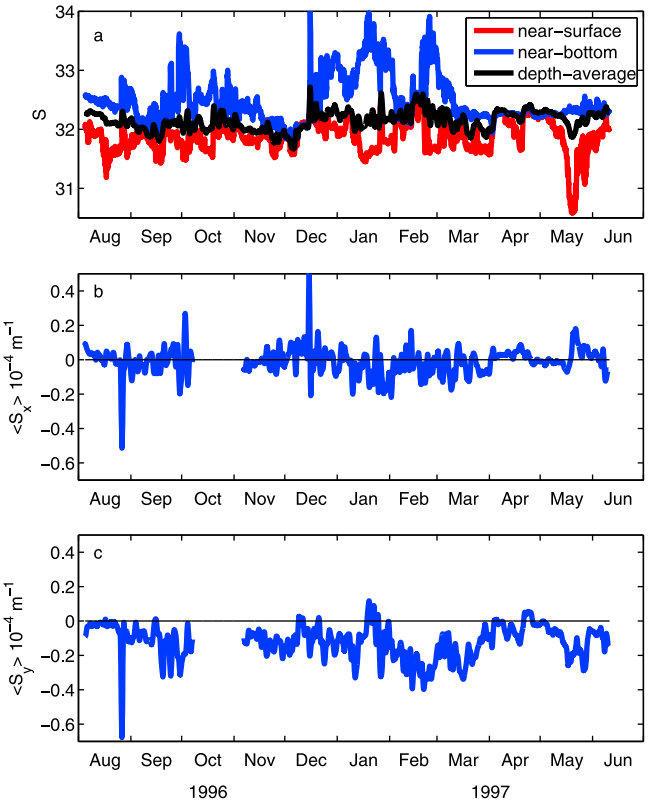

Figure 8. Time series of the (a) near-surface (red), near-bottom (blue), and depth-average (black) salinity, and the depth-average (b) along-shelf ($\langle S_x \rangle$) and (c) cross-shelf ($\langle S_y \rangle$) salinity gradients at the central site.

range from 32 to 34 (Figure 8a). Large increases in near-bottom salinity in fall and winter are associated with the onshore movement of the foot of the shelf-slope front (salinities >32.5) [e.g., *Linder and Gawarkiewicz*, 1998]. During fall and winter, there is a tendency for near-surface salinities to decrease when near-bottom salinities increase, suggesting an offshore movement of near-surface water when there is an onshore movement of near-bottom water. The foot of the shelf-slope front is present at the central site most of the time between mid December and early March due to anomalously strong and persistent eastward (upwelling-favorable) winds. In spring, there are intervals when salinities are vertically well mixed due to storms (early and late April) and near-surface low-salinity events in mid April and late May due to fresher Connecticut River plume water carried offshore and eastward by eastward winds [*Lentz et al.*, 2003a].

[32] The mean depth-average along-shelf salinity gradient ($\langle S_x \rangle$, -0.1×10^{-5} m^{-1}) is small relative to the subtidal variability (standard deviation 0.7×10^{-5} m^{-1}; Figure 8b). In contrast, there is a negative (fresher water onshore) depth-averaged cross-shelf salinity gradient ($\langle S_y \rangle$) during most of the deployment, with a few exceptions, notably in August 1996 and late April to early May 1997 when $\langle S_y \rangle$ is approximately zero (Figure 8c). The mean cross-shelf salinity gradient is -1.2×10^{-5} m^{-1}. The standard deviation (1.0×10^{-5} m^{-1}) of the subtidal variations in $\langle S_y \rangle$ is about the same magnitude as the mean. Maximum magnitudes of $\langle S_y \rangle$ are typically about -3.0×10^{-5} m^{-1} and often occur when the foot of the shelf-slope front is near the central site.

[33] There are occasional spikes in the salinity and temperature gradients associated with features that are not resolved by the coarse moored array spacing (Figures 8b, 8c, 5b, and 5c). One example is a warm salty intrusion of slope water that passed through the array in late August [see *Lentz*, 2003, Figure 1], resulting in spikes most notably in $\langle T_y \rangle$ and $\langle S_y \rangle$. The intrusion was about 40 m thick, centered at a depth of about 40 m, and had an along-shelf extent of about 10 km based on the measure along-shelf currents and the duration of the event at the central and offshore mooring sites. A second example is a near-bottom intrusion of slope water in mid December that was observed at the central mooring site but not at the along-shelf mooring site resulting in large spikes in $\langle T_x \rangle$ and $\langle S_x \rangle$. These unresolved features result in "jumps" in the cumulative advective heat and salt fluxes (see for example the mid December jump in advective heat flux divergence in Figure 7b).

3.3.2. Evaporation and Precipitation

[34] Evaporation is relatively large (≈0.5 cm day^{-1}) in fall and winter and nearly zero in late summer and spring, consistent with historical monthly means from the NCEP Reanalysis (Figure 9a). The evaporation events in fall and winter are due to offshore movement of cold dry air from the continent. During the CMO deployment, precipitation exceeds evaporation in the fall (August to October) due

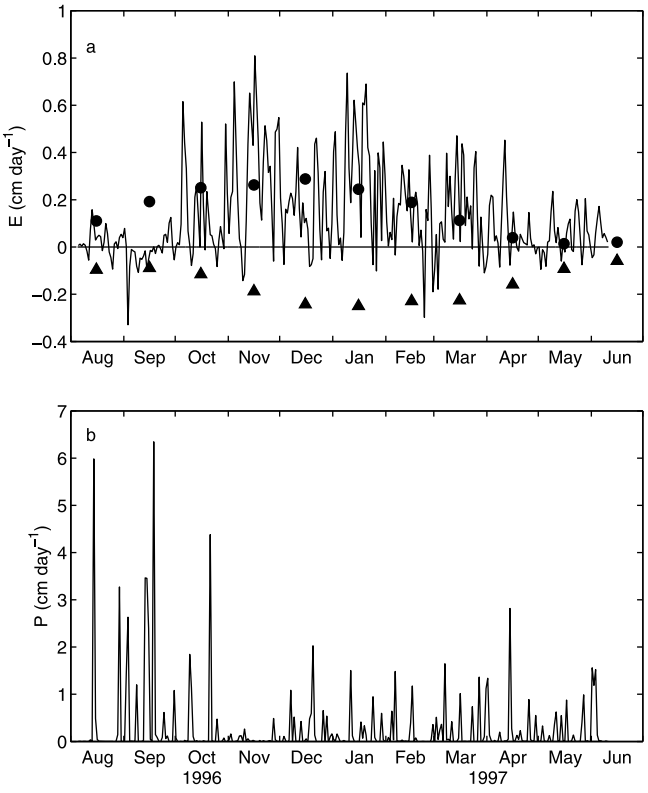

Figure 9. Time series of the daily averaged (a) evaporation (E) and (b) precipitation (P) rates at the central site. Monthly means of E (circles) and -P (triangles) from NCEP reanalysis averaged over the period 1948–2000 for a 2 degree grid square centered on 41°N 71.25°W are both shown in Figure 9a.

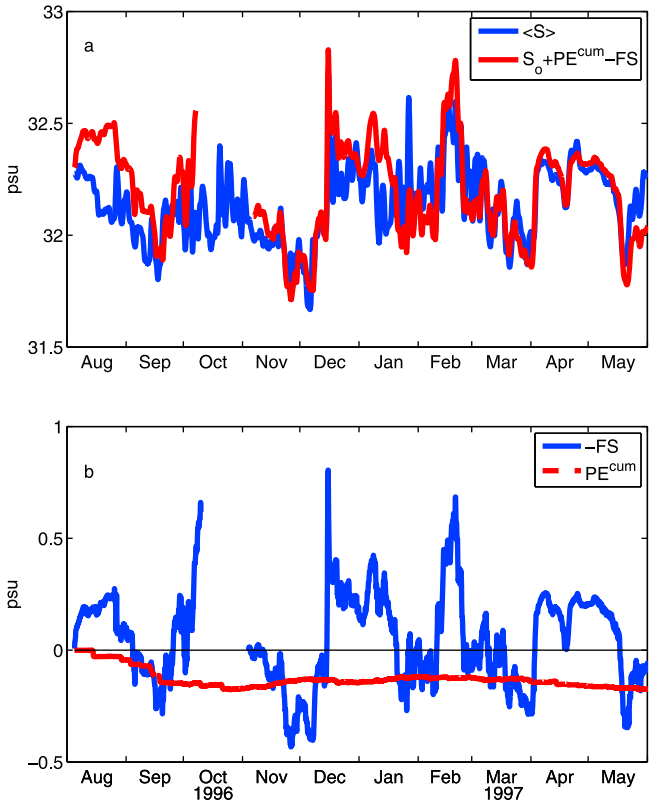

Figure 10. Time series of (a) the depth-averaged salinity ($\langle S \rangle$) at the central site (blue line) and the cumulative surface and advective flux divergence (red line) and (b) the cumulative advective salt flux divergence (blue line) and cumulative surface freshwater flux (evaporation minus precipitation; red line).

primarily to six large precipitation events (3–6 cm day^{-1}; Figure 9b). During the rest of the deployment precipitation is similar in magnitude to evaporation when averaged over time scales of weeks to months and the net freshwater surface flux is relatively small. Monthly means from the NCEP reanalysis also indicate a general tendency for evaporation and precipitation to balance so that the net surface freshwater flux is small (Figure 9a).

3.3.3. Salt Balance

[35] The estimated terms in the cumulative salt budget do not balance on time scales of months or longer unless the ad hoc salinity bias corrections are applied (Figure 3a). After applying the salinity bias corrections shown in Figure 3b, there is reasonable agreement between the observed salinity at the central site and the cumulative salt flux divergence (Figure 10a). The agreement in variations with time scales of days to weeks is not affected by the salinity bias corrections. The correlation between the depth-average salinity at the central site and the cumulative surface and advective flux divergence shown in Figure 10a is 0.73 (significant at the 95% confidence level).

[36] Advective salt flux convergences and divergences are the dominant cause of the observed depth-average salinity variability at the central site (Figure 10b). The dominant terms in the subtidal salt balance (2) (not shown), which emphasizes shorter time scales than the cumulative salt balance, are temporal changes in salinity driven by the advective salt flux divergence (correlation −0.58, regression slope −0.81 ± 0.13). Note the subtidal salt balance results are the same whether or not the salinity bias corrections are applied because only the cumulative salt balance is sensitive to the small bias errors. Evaporation and precipitation tend to balance and hence generally make a negligible contribution to the depth-average salinity variability, except in September 1996 when several large precipitation events (Figure 9b) reduce the depth-average salinity by about 0.2.

3.4. Processes Contributing to Advective Heat and Salt Flux Divergences

[37] The cumulative advective heat and salt flux divergences (Figures 7b and 10b) include substantial contributions from subtidal variability (periods of 38 hours or longer), tidal variability (periods 12–24 h), and the Stokes drift velocity associated with surface gravity waves (periods 6–12 s; Figure 11). Each of these contributions is discussed below for both heat and salt.

3.4.1. Subtidal Variability

[38] The largest contributions to the cumulative advective heat and salt flux divergence come from the subtidal variability (FT^{lf} and FS^{lf}) (Figure 11, thick lines). Two processes account for most of the subtidal heat and salt flux divergence: 1) along-shelf advection of colder water from the northeast toward the southwest by the depth-average flow, and 2)

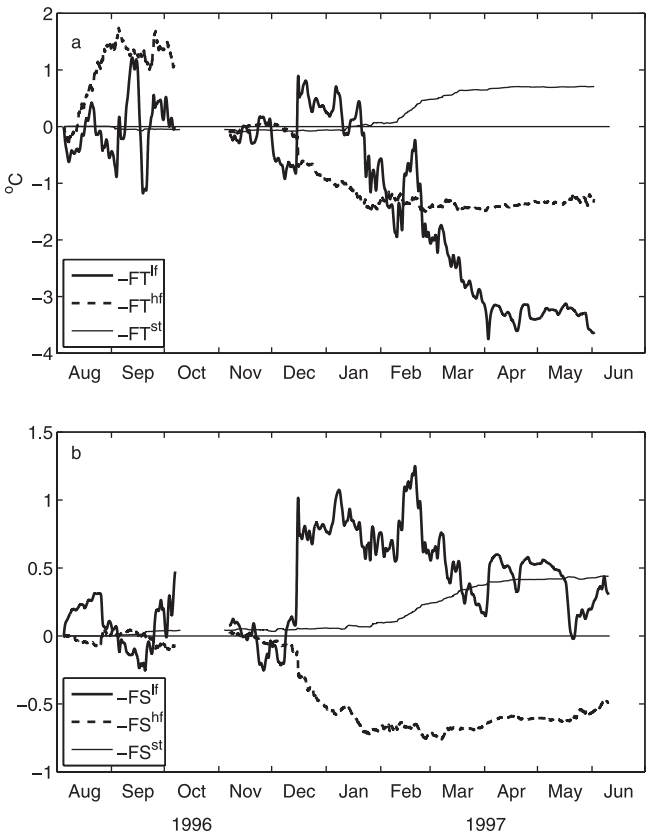

Figure 11. Advective (a) heat and (b) salt flux divergence due to the subtidal variability (F^{lf}; thick lines), tidal variability (F^{hf}; dashed lines) and surface gravity wave Stokes drift (F^{st}; thin lines).

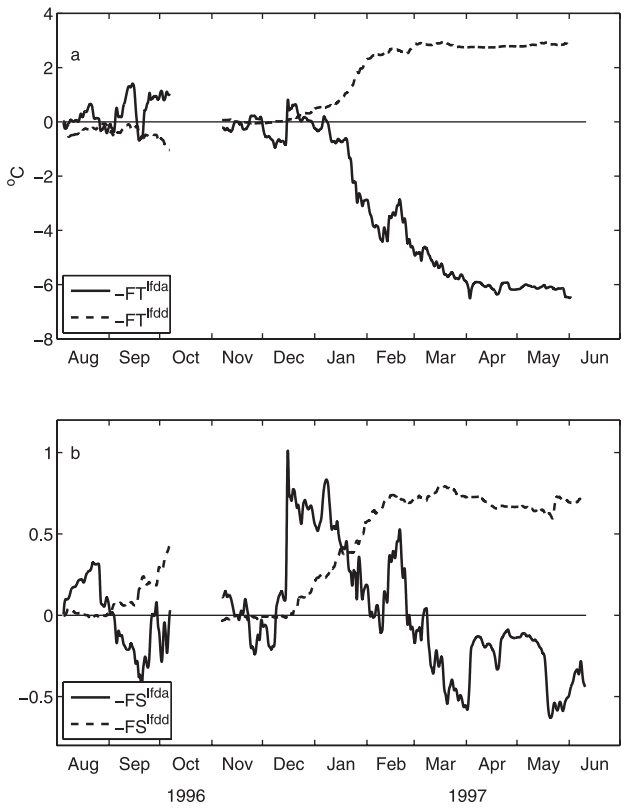

Figure 12. Advective (a) heat and (b) salt flux divergence due to the subtidal depth-average flow (solid lines) and the subtidal depth-dependent exchange flow (dashed lines).

wind-driven cross-shelf advection (coastal upwelling) that transports warmer, saltier slope water onshore near the bottom and cooler, fresher shelf offshore near the surface. To separate these two contributions, the subtidal variability is further decomposed into depth-averaged (e.g., u^{lfda}) and depth-dependent (e.g., u^{lfdd}) components. For example, $u^{lf} = u^{lfda} + u^{lfdd}$, where $u^{lfda} = \langle u^{lf} \rangle$, $u^{lfdd} = u^{lf} - u^{lfda}$, and

$$FT^{lf} = FT^{lfda} + FT^{lfdd}.$$

[39] Most of the variability in the advective heat and salt flux divergence on time scales of days to weeks is due to the subtidal depth-averaged flow (compare solid lines in Figure 12 with thick lines in Figure 11). There is also a longer time scale 6°C temperature decrease in winter (Figure 12a) due to the depth-average westward along-shelf flow (Figure 4c) acting on the weak along-shelf temperature gradient (colder water toward the northeast; Figure 5b). The corresponding salinity decrease in winter due to the depth-averaged flow (Figure 12b) is less certain because of the uncertainty associated with the bias errors (section 2.3), but it is reasonable since shelf waters also tend to be fresher toward the northeast in winter (Figure 8b) [*Linder et al.*, 2006].

[40] The heat and salt flux divergence driven by the depth-dependent exchange flow is generally negligible except for the period from mid December to mid February when the shelf-slope front is located at the CMO array site (Figure 12, dashed lines). During this period, a cross-isobath exchange flow drives an onshore transport of warm, salty slope water near the bottom and an offshore transport of cooler, fresher shelf water near the surface. The net result is an increase in the depth-averaged temperature and salinity of 3°C and 0.7, respectively. This increase in temperature and salinity partially offsets the substantial decreases in temperature and salinity from mid December to the end of March due to the depth-average flow (Figure 12, solid lines). *Lentz et al.* [2003a] show that the onshore movement of the foot of the shelf-slope front is due to anomalously strong and persistent upwelling favorable winds in the winter of 1996–1997.

3.4.2. Tidal-Band Variability

[41] The advective flux divergence due to the high-frequency (tidal) variability (periods between 2 and 38 hours) causes a 1.5°C temperature decrease and a 0.7 salinity decrease between mid December and the end of January (Figure 11, dashed lines). The high-frequency variability also causes a 1.5°C temperature increase in August. In both cases the cumulative flux divergence is due almost entirely to the depth-average tidal currents acting on the depth-average temperature and salinity gradients suggesting that baroclinic processes are not the cause of the high-frequency fluxes.

[42] Barotropic tides are the dominant source of high-frequency current variability on the New England shelf [*Shearman and Lentz*, 2004]. To determine whether the high-frequency contributions to the heat and salt flux divergence are due to the barotropic tides, a harmonic tidal analysis of the currents, temperature gradients, and salinity gradients was carried out [*Pawlowicz et al.*, 2002].

[43] Six tidal constituents (O_1, P_1, K_1, M_2, S_2, N_2) account for 92% of the high-frequency depth-average current variance, but less than 1% of the high-frequency depth-averaged temperature gradient variance and less than 3% of the high-frequency depth-averaged salinity gradient variance. Consequently, using the results of the harmonic analysis to compute the product of current and temperature gradient variability or current and salinity gradient variability results in a negligible contribution to the observed heat and salt flux divergences. In contrast, the product of tidal currents and the broad-band high-frequency temperature or salinity gradient time series (i.e., decomposing currents, but not temperature or salinity gradients into tidal constituents) accounts for the observed flux divergence due to the high-frequency variability. The flux divergences occur during periods when the high-frequency variability in the temperature or salinity gradients happens to be coherent with the barotropic tidal currents. It is unclear whether the coherence is random or a consequence of some process. It is also unclear whether this is a local phenomenon associated with along-shelf variations in the tidal response around Nantucket Shoals [*Wilkin*, 2006] or a larger scale phenomenon.

3.4.3. Surface Gravity Wave Variability

[44] Surface gravity waves are primarily directed onshore at the CMO site, and thus the cumulative advective heat and salt fluxes are dominated by the contribution of the onshore Stokes drift velocity u^{st} to the cross-shelf flux components $u^{st}T_x$ and $u^{st}S_x$. The onshore Stokes drift velocity has little impact on the heat and salt balances, except in February 1997 when the cumulative advective heat and salt flux divergences cause a temperature increase of about 0.7°C and a salinity increase of 0.4 at the central site (Figure 11, thin lines). While the Stokes drift velocity contribution to the heat balance

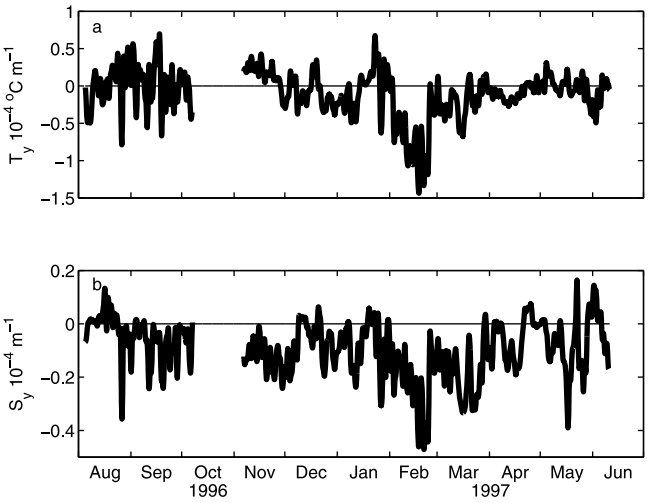

Figure 13. Near-surface cross-shelf (a) temperature and (b) salinity gradients.

is smaller than the subtidal and tidal flux divergences (Figure 11a), the contribution to the salt balance is similar in size to the subtidal and tidal flux divergences (Figure 11b). The heat and salt flux due to the Stokes drift in February is at first puzzling since the waves were not particularly large during this period relative to rest of the fall and winter (Figure 4b). The wave-driven advective flux divergence is large in February because the Stokes drift velocity is always concentrated near the surface and the near-surface cross-shelf temperature and salinity gradients, which the Stokes drift acts on, are largest in February (Figure 13).

[45] The potential role of surface gravity waves in forcing cross-shelf fluxes of heat and salt have not been considered until recently [*Fewings*, 2007]. The results presented here suggest that even over the mid to outer-shelf surface gravity waves may result in significant onshore fluxes of both heat and salt in winter in regions of strong near-surface cross-shelf gradients such as the shelf-slope front. In particular, the cumulative heat budget for CMO (Figure 7) closes less well if the surface gravity wave contribution is neglected.

[46] The net onshore heat and salt flux due to waves (in the absence of any other forcing) is the sum of the wave-driven flux (estimated using the Stokes velocity) and any flux due to the "mean" (time scales long compared to the wave period) flow driven by surface gravity waves. The flux due to the wave-driven mean flow is presumably resolved by our measurements and hence included in our estimates of the advective heat and salt flux.

[47] However, we can not determine the net onshore flux due to surface gravity waves because we are not able to isolate that portion of the observed "mean" currents due to surface gravity wave forcing. The wave-driven mean flow may be equal and opposite to the Stokes velocity as found by *Lentz et al.* [2008] over the inner shelf, resulting in no net wave-driven heat or salt flux. Clearly, a better understanding of "mean" flows driven by surface gravity waves is essential to understanding the potential role of surface gravity waves in transporting heat, salt, and other constituents. The results presented here suggest studies using fixed instruments that do not sample fast enough (1 Hz) or close enough to the surface (above the wave trough) to directly measure the wave-driven fluxes need to consider estimating the wave-driven flux using the Stokes drift velocity (as done here using equation (5)).

4. Summary

[48] The dominant terms in the depth-averaged heat and salt balances over time scales of days to months on the mid to outer New England continental shelf are determined using current, temperature, and salinity time series from a four-element moored array and meteorological observations from a surface buoy deployed between August 1996 and June 1997. Close agreement between the observed depth-average temperature and the time integral of the surface and advective heat fluxes indicates that the moored array observations provide accurate estimates of the dominant terms in the heat balance (Figure 7a). There is also close agreement between the observed depth-average salinity and the time integral of the surface and advective salt flux on time scales of days to weeks (Figure 10a), but not at longer time scales unless ad hoc salinity corrections are applied (Figure 3).

[49] Depth-average temperature variability was dominated by the annual cycle ranging from 14°C in August to 5°C in March. A large part of the annual variation was due to the surface heat flux (Figure 7b), which warmed the shelf water in spring and summer due primarily to solar radiation and cooled the shelf water in late fall and winter due to latent and sensible heat loss (Figure 6). Horizontal advection resulted in a steady cooling during the winter and a briefer warming in late summer (Figure 7b). Temperature variability on time scales of days to weeks was dominated by advective heat fluxes.

[50] Depth-average salinity variability was primarily at time scales of days to weeks and did not exhibit an obvious seasonal variation (Figure 10a). Salinity variations were almost entirely due to advection (Figure 10b). Precipitation and evaporation tended to balance so the net freshwater flux was small.

[51] Advective heat and salt flux divergences included substantial contributions from subtidal variability (periods longer than 38 hours), tidal-band variability (periods 12–24 hours), and surface gravity wave variability (periods of 6–12 s; Figure 11). The largest contribution was from the persistent depth-averaged westward along-shelf flow advecting cooler and fresher water from the northeast toward the southwest resulting in a 6°C temperature decrease and a 1.4 salinity decrease during the winter (Figure 11, thick lines). This temperature and salinity decrease was partially compensated by a wind-driven cross-shelf upwelling circulation in winter that advected warm, salty slope water onshore near the bottom and cooler, fresher shelf water offshore near the surface (Figure 11, thin lines). Correlations between barotropic along-shelf tidal currents and tidal-band variability in the along-shelf temperature and salinity gradients caused decreases in temperature of 1.5°C and salinity of 0.7 from mid December to January (Figure 11, dashed lines), when the foot of the shelf-slope front was located at the moored array site. It is unclear why the along-shelf temperature and salinity gradient tidal-band variations are coherent with the barotropic tidal currents during this period. Stokes drift associated with surface gravity waves resulted in a temperature increase of 0.7°C and a salinity increase of 0.4 in February (Figure 11, thin lines). These fluxes were large in February because the

wave-driven Stokes velocities are concentrated near the surface and this was the period when near-surface cross-shelf temperature and salinity gradients were largest at the CMO moored array site. The relatively large magnitude of the fluxes due to surface gravity waves and the accurate closure of the 10 month heat balance with Stokes drift contributions included suggest that wave-driven Stokes transports need to be considered in estimates of cross-shelf heat and salt transport.

[52] **Acknowledgments.** The design, deployment, and recovery of the moored array, the preparation of the instruments, and processing of the data were done by N. Galbraith, W. Ostrom, R. Payne, Trask, G. Tupper, J. Ware, and B. Way of the Upper Ocean Processes Group with assistance from M. Baumgartner, C. Marquette, M. Martin, N. McPhee, E. Terray, and S. Worrilow. The moorings were fabricated by the WHOI Rigging Shop under the direction of D. Simoneau. The success of the field program was a direct result of the exceptional efforts of all those involved and that effort is greatly appreciated. The field program was funded by the Office of Naval Research, Code 322, under grant N00014-95-1-0339. Analysis was also partially supported by the National Science Foundation Physical Oceanography program under grants OCE-0647050 and OCE-0548961.

References

Austin, J. A., and S. J. Lentz (1999), The relationship between synoptic weather systems and meteorological forcing on the North Carolina inner shelf, *J. Geophys. Res.*, *104*(C8), 18,159–18,186.

Beardsley, R. C. (1987), A comparison of the vector-averaging current meter and new Edgerton, Germeshausen, and Grier, Inc., vector-measuring current meter on a surface mooring in CODE 1, *J. Geophys. Res.*, *92*(C2), 1845–1860.

Beardsley, R. C., and W. C. Boicourt (1981), On estuarine and continental-shelf circulation in the Middle Atlantic Bight, in *Evolution of Physical Oceanography: Scientific Surveys in Honor of Henry Stommel*, edited by B. A. Warren and C. Wunsch, pp. 198–233, MIT Press, Cambridge, Mass.

Beardsley, R. C., R. Limeburner, and L. K. Rosenfeld (1985), Introduction to CODE-2 moored array and large-scale data report, in CODE-2 Moored Array and Large Scale Data Report, *Tech. Rep. 85–35*, edited by R. Limeburner, pp. 1–22, Woods Hole Oceanogr. Inst., Woods Hole, Mass.

Beardsley, R. C., S. J. Lentz, R. A. Weller, R. Limeburner, J. D. Irish, and J. B. Edson (2003), Surface forcing on the southern flank of Georges Bank, February–August 1995, *J. Geophys. Res.*, *108*(C11), 8007, doi:10.1029/2002JC001359.

Benway, R. L., and J. W. Jossi (1998), Departures of 1996 temperatures and salinities in the Middle Atlantic Bight and Gulf of Maine from historical means, *J. Northwest Atl. Fish. Sci.*, *24*, 61–86.

Bigelow, H. B. (1933), Studies of the waters on the continental shelf, Cape Cod to Chesapeake Bay, part I, The cycle of temperature, *Pap. Phys. Oceanogr. Meteorol.*, *2*(4), 1–135.

Bigelow, H. B., and M. Sears (1935), Studies of the waters on the continental shelf, Cape Cod to Chesapeake Bay, part II, Salinity, *Pap. Phys. Oceanogr. Meteorol.*, *4*(1), 1–94.

Bignami, F., and T. S. Hopkins (2003), Salt and heat trends in the shelf waters of the southern Middle-Atlantic Bight, *Cont. Shelf Res.*, *23*(6), 647–667.

Brink, K. H. (1998), Deep-sea forcing and exchange processes, in *The Global Coastal Ocean Processes and Methods, The Sea*, vol. 10, edited by K. H. Brink and A. R. Robinson, pp. 151–167, John Wiley, New York.

Fairall, C. W., E. F. Bradley, D. P. Rogers, J. B. Edson, and G. S. Young (1996), Bulk parameterization of air-sea fluxes for Tropical Ocean-Global Atmosphere Coupled-Ocean Atmosphere Response Experiment, *J. Geophys. Res.*, *101*(C2), 3747–3764.

Fairbanks, R. G. (1982), The origin of continental shelf and slope water in the New York Bight and Gulf of Maine: Evidence from $H_2^{18}O/H_2^{16}O$ ratio measurements, *J. Geophys. Res.*, *87*(C8), 5796–5808.

Fewings, M. R. (2007), Cross-shelf circulation and momentum and heat balances over the inner continental shelf near Martha's Vineyard, Massachusetts, Ph.D. thesis, 267 pp., Woods Hole Oceanogr. Inst. and Mass. Inst. of Technol. Jt. Program in Oceanogr./Appl. Ocean Sci. and Eng., Woods Hole, Mass.

Galbraith, N., A. Plueddemann, S. Lentz, S. Anderson, M. Baumgartner, and J. Edson (1999), Coastal Mixing and Optics Experiment moored array data report, *Tech. Rep. WHOI-99-15*, 156 pp., Woods Hole Oceanogr. Inst., Woods Hole, Mass.

Garvine, R. W., K.-C. Wong, and G. G. Gawarkiewicz (1989), Quantitative properties of shelfbreak eddies, *J. Geophys. Res.*, *94*(C10), 14,475–14,483.

Gawarkiewicz, G., K. H. Brink, F. Bahr, R. C. Beardsley, M. Caruso, J. F. Lynch, and C.-S. Chiu (2004), A large-amplitude meander of the shelfbreak front during summer south of New England: Observations from the Shelfbreak PRIMER experiment, *J. Geophys. Res.*, *109*, C03006, doi:10.1029/2002JC001468.

Houghton, R. W., F. Aikman III, and H. W. Ou (1988), Shelf-slope frontal structure and cross-shelf exchange at the New England shelf-break, *Cont. Shelf Res.*, *8*(5–7), 687–710.

Houghton, R. W., C. N. Flagg, and L. J. Pietrafesa (1994), Shelf-slope water frontal structure, motion and eddy heat flux in the southern Middle Atlantic Bight, *Deep Sea Res.*, *41*(2–3), 273–306.

Joyce, T. M. (1987), Meteorology and air-sea interactions, in *The Marine Environment of the U.S. Atlantic Continental Slope and Rise*, edited by J. D. Milliman and W. R. Wright, pp. 5–26, Jones and Bartlett, Boston.

Lentz, S. J. (2003), A climatology of salty intrusions over the continental shelf from Georges Bank to Cape Hatteras, *J. Geophys. Res.*, *108*(C10), 3326, doi:10.1029/2003JC001859.

Lentz, S. J. (2010), The mean along-isobath heat and salt balances over the Middle Atlantic Bight continental shelf, *J. Phys. Oceanogr.*, *40*, 934–948.

Lentz, S. J., K. Shearman, S. Anderson, A. Plueddemann, and J. Edson (2003a), The evolution of stratification over the New England shelf during the Coastal Mixing and Optics study, August 1996–June 1997, *J. Geophys. Res.*, *108*(C1), 3008, doi:10.1029/2001JC001121.

Lentz, S. J., R. C. Beardsley, J. D. Irish, J. Manning, P. C. Smith, and R. A. Weller (2003b), Temperature and salt balances on Georges Bank February–August 1995, *J. Geophys. Res.*, *108*(C11), 8006, doi:10.1029/2001JC001220.

Lentz, S. J., M. Fewings, P. Howd, J. Fredericks, and K. Hathaway (2008), Observations and a model of undertow over the inner continental shelf, *J. Phys. Oceanogr.*, *38*, 2341–2357.

Linder, C. A., and G. Gawarkiewicz (1998), A climatology of the shelfbreak front in the Middle Atlantic Bight, *J. Geophys. Res.*, *103*(C9), 18,405–18,423.

Linder, C. A., G. G. Gawarkiewicz, and M. Taylor (2006), Climatological estimation of environmental uncertainty over the Middle Atlantic Bight shelf and slope, *IEEE J. Oceanic Eng.*, *31*(2), 308–324.

Manning, J. (1991), Middle Atlantic Bight salinity: Interannual variability, *Cont. Shelf Res.*, *11*(2), 123–137.

Mayer, D. A., D. V. Hansen, and D. A. Ortman (1979), Long-term current and temperature observation on the Middle Atlantic shelf, *J. Geophys. Res.*, *84*(C4), 1776–1792.

Mountain, D. G., G. A. Strout, and R. C. Beardsley (1996), Surface heat flux in the Gulf of Maine, *Deep Sea Res.*, *43*(7–8), 1533–1546.

Pawlowicz, R., R. Beardsley, and S. J. Lentz (2002), Classical tidal harmonic analysis with errors in MATLAB using T_TIDE, *Comput. Geosci.*, *28*(8), 929–937.

Shearman, R. K. (2005), Observations of near-inertial current variability on the New England shelf, *J. Geophys. Res.*, *110*, C02012, doi:10.1029/2004JC002341.

Shearman, R. K., and S. J. Lentz (2003), Dynamics of mean and subtidal flow on the New England shelf, *J. Geophys. Res.*, *108*(C8), 3281, doi:10.1029/2002JC001417.

Shearman, R. K., and S. J. Lentz (2004), Observations of tidal variability on the New England shelf, *J. Geophys. Res.*, *109*, C06010, doi:10.1029/2003JC001972.

Smith, P. C., R. W. Houghton, R. G. Fairbanks, and D. G. Mountain (2001), Interannual variability of boundary fluxes and water mass properties in the Gulf of Maine and on Georges Bank: 1993–1997, *Deep Sea Res.*, *48*(1–3), 37–70.

Weller, R. A., and R. E. Davis (1980), A vector-measuring current meter, *Deep Sea Res.*, *27*(7), 575–582.

Wilkin, J. L. (2006), The summertime heat budget and circulation of southeast New England shelf waters, *J. Phys. Oceanogr.*, *36*, 1997–2011.

Wright, W. R. (1976), The limits of shelf water south of Cape Cod, 1941 to 1972, *J. Mar. Res.*, *34*(1), 1–14.

S. J. Lentz, Department of Physical Oceanography, Woods Hole Oceanographic Institution, Mail Stop 21, Woods Hole, MA 02543, USA. (slentz@whoi.edu)

A. J. Plueddemann, Department of Physical Oceanography, Woods Hole Oceanographic Institution, Mail Stop 29, Woods Hole, MA 02543, USA. (aplueddemann@whoi.edu)

R. K. Shearman, College of Oceanic and Atmospheric Sciences, Oregon State University, 104 COAS Administration Building, Corvallis, OR 97331, USA. (shearman@coas.oregonstate.edu)